INSTITUTE OF PHYSICS PUBLISHING NANOTECHNOLOGY
Nanotechnology **17** (2006) 3655–3661 doi:10.1088/0957-4484/17/15/006

The growth mechanism and field-emission properties of single carbon nanotips

K S Yeong[1], C B Boothroyd[2] and J T L Thong[1]

[1] Department of Electrical and Computer Engineering, National University of Singapore, 4 Engineering Drive 3, Singapore 117576, Singapore
[2] Institute of Materials Research and Engineering, 3 Research Link, Singapore 117602, Singapore

E-mail: elettl@nus.edu.sg

Received 8 May 2006, in final form 1 June 2006
Published 27 June 2006
Online at stacks.iop.org/Nano/17/3655

Abstract
We study the self-aligned growth of a single carbon nanotip on a sharp metal tip via the field-emission-induced growth method. Under typical growth conditions, a micron long nanotip can be formed in around 10 s by field emission in the presence of acetylene gas at $\sim 10^{-2}$ mbar. The tip radius of the carbon nanotip can be as small as 5 nm, while its length is determined by the growth duration. Electron energy loss spectroscopy (EELS) analysis in a transmission electron microscope revealed that the carbon nanotip is amorphous carbon with predominant sp^2 bonding. The growth mechanism of the carbon nanotip is discussed to explain the formation of the nanotip and its carbon matrix. Field-emission measurements showed that emission from the carbon nanotip follows the Fowler–Nordheim equation, suggesting that the tip shows metallic behaviour as far as field emission is concerned. A high emission current stress cycle is found to improve the emission current stability significantly.

1. Introduction

Carbon nanotips or nanocones have a variety of applications such as field emitters, scanning probe microscope tips, and nanoindenters, mainly due to the chemical inertness of the carbon surface, typically small tip radii, and much higher bending stiffness compared to carbon nanotubes of otherwise comparable tip curvature. To date, a considerable number of studies have been reported concerning the growth and application of carbon nanotips. Different growth methods for fabricating carbon nanotips include such techniques as electron-beam-induced deposition (EBID) [1–3] and its focused-ion-beam counterpart [4], chemical vapour deposition (CVD) [5–7], and plasma-enhanced chemical deposition (PECVD) [8]. These methods give rise to a variety of carbon structures ranging from amorphous to crystalline. CVD methods have been used to grow arrays of carbon nanotips on flat substrates for field-emission studies [9, 10]. However, in order to study the properties of a carbon nanotip as a single field emitter, a probe tip, or a nanoindenter, it needs to be incorporated into a useful device, which often entails growing or mounting a single carbon tip on a sharp tip or pedestal. If multiple carbon nanotip/nanocones were first grown on a substrate, further assembly processes that are often tedious are needed to mount an individual cone. On the other hand, EBID is able to grow a single nanotip at the desired location for such applications; however, EBID is a slow growth process which usually requires typically hundreds of seconds to obtain a high-aspect-ratio carbon nanotip. A long deposition time often leads to asymmetry in the deposited tip due to drift and defocus of the electron beam, and thus periodic refocusing may be required during growth [1–3].

In this paper, we study the growth of a single carbon nanotip on a sharp metal tip through field-emission-induced growth (FEIG) [11, 12]. The growth method is simple, controllable, and has a much higher deposition rate compared to EBID. The growth mechanism of the carbon nanotip is discussed to explain the formation of the nanotip and its amorphous carbon matrix with the aid of electrostatic simulations. One of the advantages of the method is that the nanotip is ready for use without the need for further assembly. The grown tip is also mechanically well-anchored and self-aligned to the underlying metal tip. A field-emission study has also been performed to explore its potential as a cold-field-emission cathode.

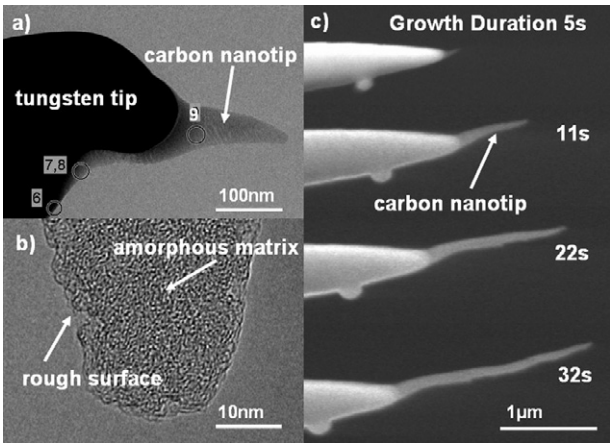

Figure 1. (a) TEM image of FEIG carbon nanotip grown on a sharp tungsten tip for TEM analysis. (b) High-resolution image of the nanotip. (c) SEM pictures of a carbon nanotip taken at 5, 11, 22, and 32 s from the start of field emission.

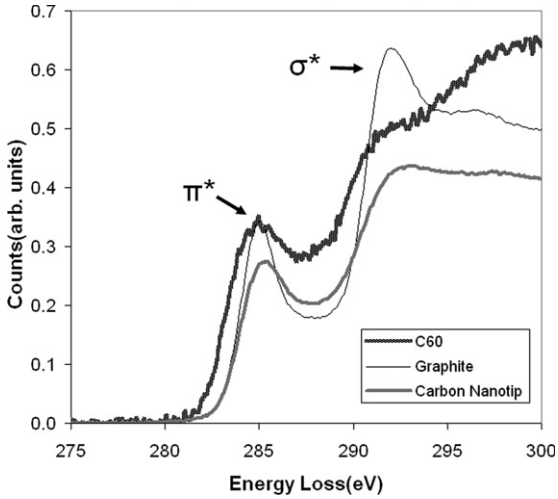

Figure 2. Energy loss spectra from the carbon nanotip at region 9, C_{60} and graphite samples taken using a Phillips CM300 equipped with a Gatan imaging filter. The C_{60} and graphite spectra have been rescaled to have the same y-axis.

2. Growth process and characterization

The carbon nanotip was grown in the specimen chamber of a Philips XL30 FEG environmental scanning electron microscope (ESEM). Two electrochemically etched tungsten tips were positioned by nanomanipulators such that they faced each other, serving as cathode and anode tips separated by 10 μm. Acetylene was used as the carbon source, and was admitted into the chamber through a dosing valve and a nozzle directed at the two tips; the gas flow rate was controlled by monitoring the specimen chamber pressure. Field emission from the cathode was then initiated by applying an anode bias. The interaction of field-emitted electrons with the acetylene molecules generates hydrocarbon ions. These hydrocarbon ions are directed by the electric field towards the cathode tip where they deposit as a nanotip, which then becomes the field-emission tip and growth front. The growth mechanism will be discussed in detail in section 3.

Figures 1(a) and (b) show a carbon nanotip grown for transmission electron microscope (TEM) analysis. The field-emission current during growth was 300 nA, while the chamber pressure was set to 2.0×10^{-4} mbar, from which the local vapour pressure in the vicinity of the nozzle was estimated to be about 10^{-2} mbar based on the pumping speed of the vacuum system and the nozzle geometry. Figure 1(c) shows micrographs of a carbon nanotip grown at 500 nA, 2.2×10^{-4} mbar taken at different times from the initiation of field emission. The length of the carbon nanotip was found to increase almost linearly with time, with a growth rate of 4.86 μm min^{-1}. The growth rate is about 50 times higher than that attained with EBID methods which have typical deposition rates of 0.1 μm min^{-1} [3]. The constant emission current was sourced from a Keithley model 237 high-voltage source-measurement unit (SMU) used to bias the anode. During the growth, the anode voltage to maintain the constant growth current decreased gradually from about 1100 V to less than 400 V, and provided an indication that the carbon nanotip was growing. As the nanotip first initiates, then grows, the cathode cone angle and tip radius reduce and thus increase the field enhancement factor of the cathode which results in a gradual decrease of the anode bias voltage.

TEM analysis shows the FEIG grown carbon nanotip tip radius (r) to be around 10 nm. As shown in figure 1(b), the tip has an amorphous matrix and rough surface structure. The carbon nanotip base overcoats and merges smoothly with the underlying metal tip. The carbon K-edge electron energy loss spectrum (EELS) data from the nanotip at region 9 indicated in figure 1(a) shows a sharp peak at 285 eV and a broader peak at 293 eV (figure 2). The 285 eV peak is due to the excitation of carbon 1s electrons to the pπ^* states of sp^2 sites whereas the 293 eV peak is due to the excitation of carbon 1s electrons to the σ^* states of sp^2 or sp^3 sites. The well-resolved pπ^* peak at 285 eV suggests that the specimen is rich in sp^2 bonds [13–17]. The EEL spectrum was then compared with the EEL spectra from 100% sp^2-bonded standard samples (C_{60} and graphite) to derive the sp^2 fraction. Although the bonds in C_{60} are not strictly 100% sp^2, this has been shown to have minimal effect on the sp^2 fractions calculated [18]. The graphite used was polycrystalline and randomly oriented, thus averaging out the anisotropy in graphite EEL spectra with respect to beam direction and providing a good approximation to the random orientation of the sp^2 bonds in the carbon nanotip. All the EEL spectra acquired were compensated with respect to their exposure time and sample thickness in order to obtain an accurate estimate. The sp^2 fraction of the amorphous matrix can be derived from [16],

$$sp^2 = \frac{U_{\pi^*}}{U_{\pi^*+\sigma^*}} \times \frac{S_{\pi^*+\sigma^*}}{S_{\pi^*}} \qquad (1)$$

where U represents the unknown sample and S represents the standard sample. π^* and σ^* are the integrated areas that we had chosen between 283–287 and 291–295 eV. The results showed that the FEIG carbon nanotip possesses an sp^2 fraction of about 91%, which suggests a small percentage of sp^3 bonds.

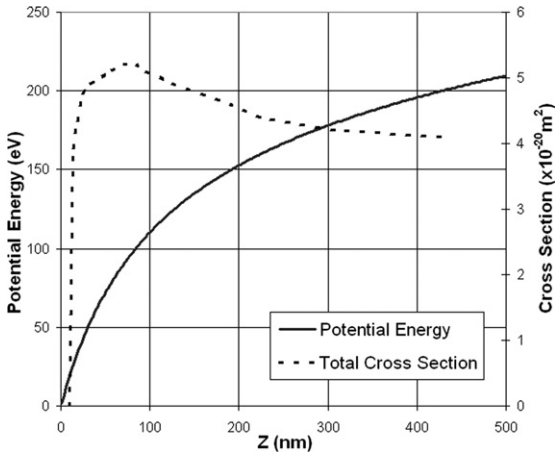

Figure 3. Field-emitted electron potential energy profile versus axial distance from tungsten tip apex. Total ionization cross-section of C_2H_2 as a function of electron energy/potential energy, re-plotted from [14].

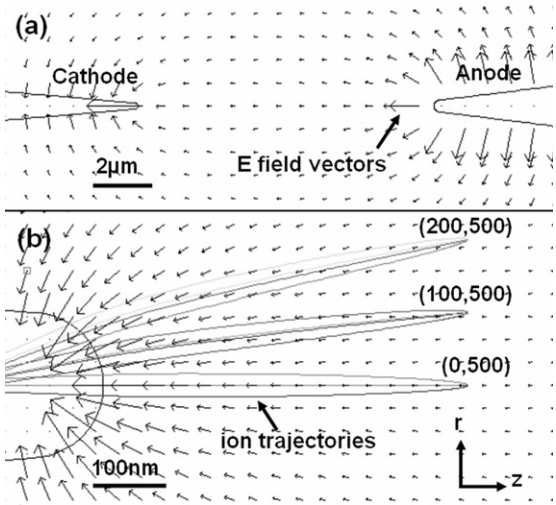

Figure 4. (a) Global electric-field distribution across anode–cathode gap. (b) Trajectories of $C_2H_2^+$ launched in different directions and from different positions relative to the cathode.

3. Growth mechanism

The growth mechanism of the FEIG carbon nanotip is further developed from the growth model of FEIG tungsten nanowire discussed by Oon *et al* [12]. The growth mechanism involves three processes: (i) the generation of hydrocarbon ions, (ii) the trajectory of the ions toward the cathode tip, and (iii) the deposition of hydrocarbon ions on the cathode surface.

The first process generates hydrocarbon ions from electron impact with acetylene molecules. Inelastic collisions cause ionization and dissociation of C_2H_2 molecules into $C_2H_2^+$, C_2H^+, C^{2+}, H^+, and other charged and uncharged species. The production of $C_2H_2^+$ is the most prolific compared to other ionic species since it possesses much higher electron-impact ionization cross-section and the lowest threshold ionization energy of 10 eV [14]; as such, we neglect the other ionic species and molecular fragmentation. The average emission electron density in the vicinity of the tip ($n_e \sim 10^{18}$ m^{-3}) at 300 nA emission/growth current is estimated to be two orders of magnitude lower than the concentration of acetylene molecules ($n_{ace} \sim 10^{20}$ m^{-3}) which ensures that the C_2H_2 concentration is not significantly depleted as a result of electron impact. This represents a different growth mode from the precursor supply-limited growth mode of tungsten nanowires considered by Oon *et al* [12].

The generated hydrocarbon ion flux (I_+) or amount of ions generated per second is [19]

$$I_+ = n_{ace}\sigma\lambda I_e \tag{2}$$

where n_{ace} is about 10^{20} m^{-3} at a local pressure of 10^{-2} mbar, and σ is the total electron–acetylene electron-impact cross-section as shown in figure 3. The total ionization cross-section of C_2H_2 increases rapidly beyond 10 eV and peaks at an electron energy of about 100 eV before it decreases gradually at higher energies [20]. This peak in the ionization cross-section profile corresponds to the energy of field-emitted electrons would have acquired after travelling around 100 nm away from the emitter surface as illustrated in figure 3. λ is the interaction distance travelled by the electron beam. I_e is the electron beam flux or number of electrons per second. In this case, the electron flux can be modelled as an electron beam with a diverging angle of about 120° from the cathode axis [21]. The electron concentration (n_e) within each slice of the beam cone is not a constant but exhibits a narrow Gaussian distribution across the ±60°.

Thus, hydrocarbon ions are generated starting from a distance very close to the emitter surface that is about 10 nm, corresponding to the threshold ionization energy to create $C_2H_2^+$. Beyond this, the local hydrocarbon ion generation rate increases rapidly, and peaks at around 100 nm before decreasing at greater distances. The radial distribution of the local hydrocarbon ion generation rate may be expected to follow the Gaussian distribution of n_e. Hence, it is clear that the highest ion generation rate is from the interaction volume right in front of the emission tip.

The second process involves the trajectory of the hydrocarbon ions (mostly $C_2H_2^+$) being accelerated and directed by the intense electric field towards the cathode. The ion trajectory will reveal where most of the hydrocarbon ions that contribute to the carbon nanotip growth are generated from. Electrostatic and trajectory simulation is performed using the Charged Particle Optics CPO-2DS program with cylindrical symmetry and a well-defined cathode and anode geometry that resembles the actual growth configuration. The simulated electric-field distribution across the cathode–anode gap and the trajectories of three $C_2H_2^+$ groups launched at different positions {($r = 0$, $z = 500$ nm); ($r = 100$ nm, $z = 500$ nm); ($r = 200$ nm, $z = 500$ nm)} near the emitter tip are shown in figure 4. Each group of $C_2H_2^+$ ions is launched assuming an initial speed v_{th} corresponding to the thermal energy ($1.5kT$) at room temperature, and at different angles with velocity $(v_r, v_z) = (v_{th}, 0)$, $(-v_{th}, 0)$, $(0, v_{th})$ and $(0, -v_{th})$. The mean free path at 10^{-2} mbar is two orders of magnitude larger than the anode–cathode gap of 10 μm. Along the trajectory towards the cathode, the $C_2H_2^+$ ions are unlikely to be ionized further, although the interaction cross-section is expected to be much higher now. This is due to considerably

higher ionization energy required for subsequent ionization and the decreasing electron energy as the ions approach the cathode.

The simulation shows that the initial velocity of the ions has relatively small impact on the future trajectory in the intense electric field. However, the location where ions were launched plays an important role as the $C_2H_2^+$ trajectory is determined by the direction of the local electric field. The ions will be directed almost immediately to follow the local electric field vector at the point of generation and at the same time accelerated along the electric field to high kinetic energy. Hence, the initial ion trajectories follow the local electric field at the point of generation and then continue roughly along this direction towards the cathode.

As shown in figure 4, ions launched at positions spanning ($r = 0$, $z = 500$ nm) and ($r = 200$ nm, $z = 500$ nm) will land close to the axis on the emitting cathode surface and contribute mainly to the growth of the carbon nanotip, whereas ions launched at larger radial distances will progressively land further back on the cathode tip and its shank. Thus, from the simulation, we can deduce that most of the hydrocarbon ions that deposit to form the carbon nanotip are generated from an interaction volume in the vicinity of the emission tip, which coincides with the interaction volume of the highest ion generation rate. We shall call this interaction volume the primary interaction volume. For ions generated far away from the emitter, only those generated along the axis contribute to the nanotip growth—those generated from the radial tails of the Gaussian distribution will just land further down on the shank of the tungsten tip.

The third process concerns the deposition of hydrocarbon ions on the cathode surface which determines the structural properties of the deposited carbon film. Reported growth models for the formation of diamond and diamond-like carbon such as the subplantation model or the preferential-sputtering model suggest that the microscopic structure of a deposited carbon film depends on the energy of the hydrocarbon ions impinging on the deposition substrate. Diamond-like carbon films exhibit the highest dominant sp^3 fraction at a hydrocarbon ion energy of 100 eV per carbon atom, while the sp^2 fraction becomes dominant towards lower or higher ion energies [22–26].

In the case of FEIG carbon nanotips, hydrocarbon ions that land on the cathode surface to form the nanotip are believed to originate mainly from the primary interaction volume as discussed above. As a result, the majority of the hydrocarbon ions landing on cathode surface have very low energies, except for ions generated far away along the axis. Low-energy ions will simply stick on the cathode surface and remain as sp^2 amorphous carbon. The high tensile stress experienced by the emitting tip during field emission may further impede the formation of sp^3 sites since compressive stress plays a significant role in facilitating sp^3 site nucleation [27–29]. A considerable amount of hydrogen atoms from the hydrocarbon ions will be buried and incorporated into the amorphous carbon matrix. Thus, the deposited carbon is likely to be hydrogenated sp^2 amorphous carbon.

An additional mechanism that may come into play is the dissociation of C_2H_2 molecules adsorbed on the cathode surface as a result of hydrocarbon ion bombardment, in a manner analogous to focused-ion-beam deposition. The amount of C_2H_2 molecules adsorbed on the emission surface is plentiful at the local pressure of 10^{-2} mbar, suggesting that this may be an important factor in contributing to the carbon nanotip growth.

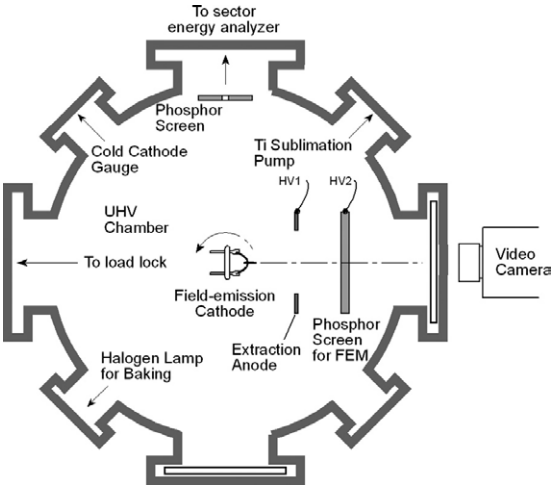

Figure 5. Field-emission characterization system.

From the above considerations, the evolution of the nanotip shape can be explained as follows. The majority of the returning ions close to the axis originate from the primary interaction volume just ahead of the emitting tip. The ion trajectories closely follow the electric field lines which are directed towards the tip, and hence the radially distributed ion flux will focus on the conical tungsten tip to result in a conical deposit. Since the landing energy of the ions is low, they deposit as an sp^2 amorphous matrix. As the cone forms, the emitting tip becomes smaller, further confining the primary interaction volume to its vicinity. Hence, this results in an even smaller tip as the cone grows until a steady-state deposition profile is achieved at which point the growing nanotip radius has reached its minimum size, limited by the threshold energy for C_2H_2 ionization.

4. Field-emission studies

Field emission from carbon fibres has been investigated since the 1970s. Baker *et al* discovered that the emission current from carbon fibres was fairly stable even at pressures of 5×10^{-7} Torr [30]. Since then, there has been growing research interest in studying the field emission from different conical carbon structures such as electrochemically-etched carbon fibre microtips [31–33], EBID carbon nanotips [1, 2], and CVD-grown carbon nanotip arrays [9, 10]. Here we performed preliminary field-emission studies of FEIG carbon nanotips.

The field-emission characterization system is shown in figure 5. The chamber has a titanium sublimation pump in addition to a dual-stage turbo-pump backed by a dry pump, and is capable of achieving a base pressure of 10^{-10} mbar. The carbon nanotip field emitter is loaded via a load-lock onto a rotatable stage at the centre of the chamber, facing a hole-extraction anode and a phosphor

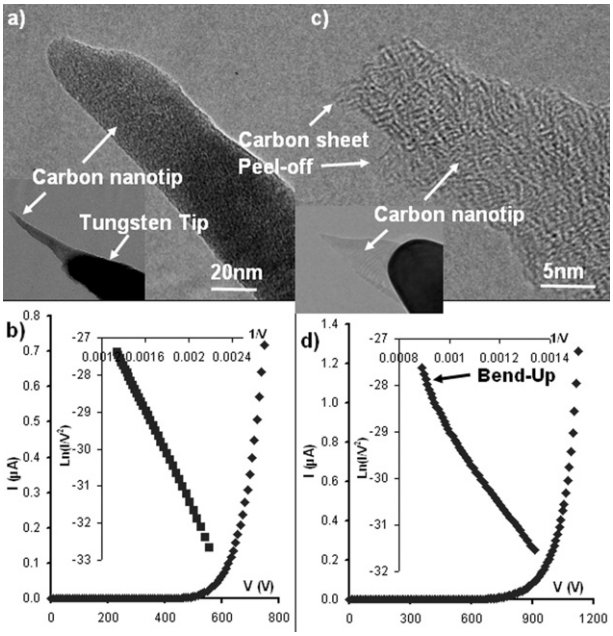

Figure 6. (a) TEM image of carbon nanotip grown for 10 s at 300 nA. The inset shows the entire nanotip. (b) I–V characteristic of the carbon nanotip shown in (a). The inset is the respective FN plot. (c) TEM image of smaller carbon nanotip, showing carbon sheet peel-off after high current density emission. (d) I–V characteristic of the carbon nanotip shown in (c). The FN plot shows deviation from the linear FN relationship in the high current region.

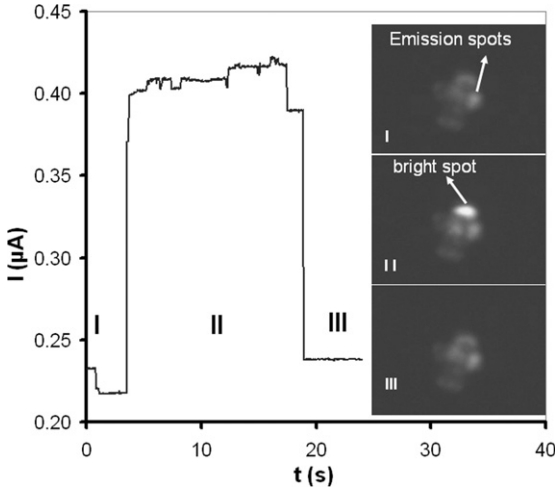

Figure 7. FEM pattern of carbon nanotip shown in figure 6(a) with respect to the emission-current changes.

screen. The setup has the ability to perform current–voltage (I–V) measurements, current stability (I–t) measurements, field-emission microscope (FEM) imaging, and field electron energy distribution (FEED) measurements with a sector energy analyser (CSA 200, Focus Electronics). All data acquisition is carried out under computer control. FEM images are recorded using a digital video camera recorder at 30 fps.

The carbon nanotip grown for field-emission studies is shown in figure 6(a); the tip radius is about 12 nm while the entire cone is 450 nm high. The current–voltage behaviour of the carbon nanotip is shown is figure 6(b). The current (I) shows an exponential relationship to anode bias voltage (V), as expected for field emission from a metallic surface following the Fowler–Nordheim (FN) equation,

$$I = A\frac{1.54\times10^{-6}E^2}{\phi}\exp\left(\frac{-6.83\times10^{7}\phi^{3/2}f(y)}{E}\right) \quad (3)$$

where the local electric field $E = \beta V$, where β is the field-enhancement factor, A is emission area, ϕ is the work function, and $f(y)$ is a function that takes into account the influence of the image force; $f(y) \sim 1$ at the field strengths and work function encountered in our experiment [20].

The derivative of equation (3) gives the well-known FN plot:

$$\frac{\mathrm{d}\ln(\frac{I}{V^2})}{\mathrm{d}(\frac{1}{V})} = \frac{-6.83\times10^{7}\phi^{\frac{3}{2}}}{\beta}. \quad (4)$$

The FN plot of the carbon nanotip up to moderate current density shows a linear relationship (inset of figure 6(b)), implying that the carbon nanotip behaves like a metallic emitter.

The emission current of the carbon nanotip shown in figure 6(a) showed step jumps and current-spike emission noise (figure 7). Step jumps are typical of emission noise exhibited by nanometre-sized emitter tips, due to the dynamics of adsorbate molecules and surface atoms, and sometimes structural changes in the emission tip [34–36]. Current-spike emission noise is usually linked to the bombardment of the emitter surface by ions formed from residual gases [37]. The field-emission pattern consists of irregularly shaped emission spots, implying a non-homogeneous current density on the emission surface which is consistent with the surface structure of a carbon nanotip that is full of nanometre-sized projections. These protrusions possess a higher field-enhancement factor and thus exhibit higher localized emission. Emission-current step jumps coincide with the appearance and disappearance of bright emission spots on the background FEM pattern, as shown in figure 8. In this case, the bright emission spot is likely to be due to an adsorbate molecule on a surface projection. Upon desorption, the bright spot disappears.

The emission-current stability was found to improve significantly after a high-current–stress cycle of about 2 μA for 2 h. Following this, the emission current was reduced to ~0.14 μA. The standard deviation of the emission noise reduced from 42.2% to 3% over the 20 min stability test period, as shown in figure 8. The FEM pattern was observed to be more uniform, suggesting a more homogeneous field-emitting surface after the current–stress cycle.

One possible explanation for the different characteristics is the change brought about by resistive heating at the emitting tip during high-current stressing as observed for an FEIG carbon nanotip with a smaller tip radius. An FN plot of a 4 nm tip radius carbon nanotip shows deviation from the ideal FN relation at higher currents, as shown in figure 6(d), similar to FN plots of CVD-grown multi-walled carbon nanotubes [38–40]. The noticeable bending-up of the carbon nanotip FN plot in the high-current region suggests that the nanotip tip has heated significantly during emission due to Joule heating. For such an obvious deviation from an ideal FN plot, the temperature rise could be up to 2000 K [37]. The

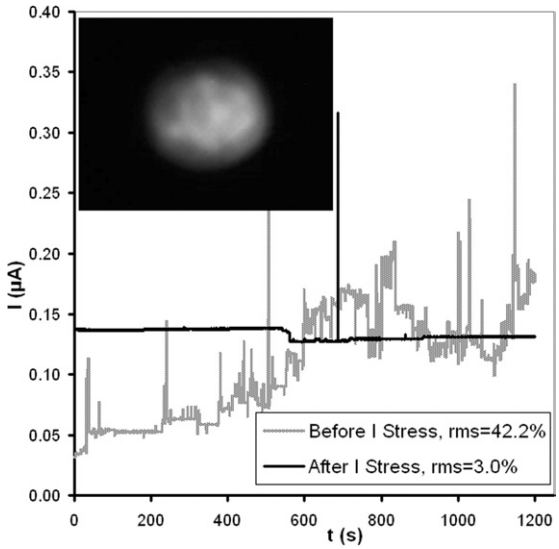

Figure 8. Emission-current stability of carbon nanotip at constant voltage bias of 550 V before and after high-current stress. The inset shown the FEM pattern after high-current stress.

combined result of the high temperature and intense electric field caused the peeling of a carbon sheet from the field-emission region as shown in figure 6(c).

However, for the carbon nanotip that had undergone the high-current–stress cycle (2 μA), a much more gentle resistive heating of the field-emitting tip would be expected since it is larger. Thus, the mild heating during the current stress cycle desorbed loosely bound adsorbate molecules and thereby improved its emission-current stability. The emission-current stability at lower current was found to degrade after several hours of ensuing field emission due to adsorption of new molecules on the emission surface. Another possible explanation that may account for the change in emission properties after the current–stress cycle is the temperature-enhanced evolution of impurity atoms such as hydrogen from the amorphous carbon matrix, and thus promote the development of carbon–carbon bonds as observed in the hydrogenated amorphous carbon matrix at temperatures as low as 350 °C [41]. This will improve surface atomic bonding and thus reduce electric-field or current-induced surface atom diffusion on the emission surface.

5. Conclusions

Single carbon nanotips were grown from acetylene using the FEIG technique on a sharp metallic tip. From EELS analysis, the carbon nanotip is largely constituted of sp^2 amorphous carbon. The growth mechanism is discussed to explain the formation of the nanotip and sp^2 amorphous matrix. The FN plot derived for field emission from the carbon nanotip is typical of a metallic emitter. An emission-current–stress cycle improved the emission-current stability significantly, suggesting potential application of such carbon nanotips as field emitters and scanning tunnelling microscope (STM) probes for use in UHV.

Acknowledgments

This project is supported by an NUS research grant R-263-000-250-112 and a grant from A*STAR.

References

[1] Adachi H, Nakane H and Katamoto M 1994 *Appl. Surf. Sci.* **76/77** 11
[2] Johnson S D, Hasko D G, Teo K B K, Milne W I and Ahmed H 2002 *Microelectron. Eng.* **61/62** 665
[3] Akama Y, Nishimura E, Sakai A and Murakami H 1990 *J. Vac. Sci. Technol.* A **8** 429
[4] Fujita J, Ishida M, Sakamoto T, Ochiai Y, Kaito T and Matsui S 2001 *J. Vac. Sci. Technol.* B **19** 2834
[5] Zhang G Y, Jiang X and Wang E G 2003 *Science* **300** 472
[6] Mani R C, Li X, Sunkara M K and Rajan K 2003 *Nano Lett.* **3** 671
[7] Li J J, Gu C Z, Wang Q, Xu P, Wang Z L, Xu Z and Bai X D 2005 *Appl. Phys. Lett.* **87** 143107
[8] Baylor L R, Merkulov V I, Ellis E D, Guillorn M A, Lowndes D H, Melechko A V, Simpson M L and Whealton J H 2002 *J. Appl. Phys.* **91** 4602
[9] Tsai C L, Chen C F and Wu L K 2002 *Appl. Phys. Lett.* **81** 721
[10] Huang C J, Chih Y K, Hwang J, Lee A P and Kou C S 2003 *J. Appl. Phys* **94** 6796
[11] Thong J T L, Oon C H, Yeadon M and Zhang W D 2002 *Appl. Phys. Lett.* **81** 4823
[12] Oon C H, Khong S H, Boothroyd C B and Thong J T L 2006 *J. Appl. Phys.* **99** 064309
[13] Waidmann S, Knupfer M, Fink J, Kleinsorge B and Robertson J 2001 *J. Appl. Phys.* **89** 3783
[14] Liang S, Yajima A, Abe S, Mera Y and Maeda K 2005 *Surf. Sci.* **593** 161
[15] Ponsonnet L, Donnet C, Varlot K, Martin J M, Grill A and Patel V 1998 *Thin Solid Films* **319** 97
[16] Silva S R P and Stolojan V 2005 *Thin Solid Films* **488** 283
[17] Ferrari A C, Libassi A, Tanner B K, Stolojan V, Yuan J, Brown L M, Rodil S E, Kleinsorge B and Robertson J 2000 *Phys. Rev.* B **62** 11089
[18] Papworth A J, Keily C J, Burden A P, Silva S R P and Amaratunga G A J 2000 *Phys. Rev.* B **62** 12628
[19] McDaniel E W 1964 *Collision Phenomena in Ionized Gases* (New York: Wiley)
[20] Zheng S H and Srivastava S K 1996 *J. Phys. B: At. Mol. Opt. Phys* **29** 3235
[21] Dyke W P and Dolan W W 1956 Field emission *Advances in Electronics and Electron Physics* vol VIII (New York: Academic) pp 90–182
[22] Zou J W, Schmidt K, Reichelt K and Dischler B 1990 *J. Appl. Phys.* **67** 487
[23] Robertson J 1994 *Diamond Relat. Mater.* **3** 361
[24] Robertson J 1993 *Diamond Relat. Mater.* **2** 984
[25] Merkulov V I, Lowndes D H, Jellison G E Jr, Puretzky A A and Geohegan D B 1998 *Appl. Phys. Lett.* **73** 2591
[26] Fallon P J, Veerasamy V S, Davis C A, Robertson J, Amaratunga C A J, Milne W I and Koskinen J 1993 *Phys. Rev.* B **48** 4777
[27] McKenzie D R, Muller D and Pailthorpe B A 1991 *Phys. Rev. Lett.* **67** 773
[28] McKenzie D R and Bilek M M M 1998 *J. Vac. Sci. Technol.* A **16** 2733
[29] Davis C A 1993 *Thin Solid Films* **226** 30
[30] Baker F S, Osborn A R and Williams J 1972 *Nature* **239** 96
[31] Hosoki S, Yamamoto S, Futamoto M and Fukuhara S 1979 *Surf. Sci.* **86** 723
[32] Mousa M S 1998 *Ultramicroscopy* **73** 23
[33] Mousa M S, Hagmann M J, Brugat M and Sheshin E P 2003 *Ultramicroscopy* **95** 119

[34] Rinzler A G, Hafner J H, Nikolaev P, Lou L, Kim S G, Tomanek D, Nordlander P, Colbert D T and Smalley R E 1995 *Science* **269** 1550
[35] Binh V T, Garcia N and Purcell S T 1996 Electron field emission from atom-sources: fabrication, properties, and applications of nanotips *Advances in Imaging and Electron Physics* vol 95 (New York: Academic) pp 63–150
[36] Hata K, Takakura A and Saito Y 2001 *Surf. Sci.* **490** 296
[37] Ashihara K, Nakane H and Adachi H 1998 *J. Vac. Sci. Technol.* B **16** 1180
[38] Purcell S T, Vincent P, Journet C and Binh V T 2002 *Phys. Rev. Lett.* **88** 105502
[39] Yeong K S and Thong J T L 2004 *Appl. Surf. Sci.* **233** 20
[40] Sveningsson M, Hansen K, Svensson K, Olsson E and Campbell E E B 2005 *Phys. Rev.* B **72** 085429
[41] Wild Ch and Koidl P 1987 *Appl. Phys. Lett.* **51** 1506